Article:
Qiao, L. orcid.org/0009-0005-0438-2717, Tang, H. orcid.org/0000-0002-2924-0126 and Huang, G. orcid.org/0000-0002-8692-7856 (2025) Persistent 2024 warm-season marine heatwave in the Kuroshio extension region under global warming. Geophysical Research Letters, 52 (16). e2025GL117274. ISSN: 0094-8276

https://doi.org/10.1029/2025gl117274

AGU ADVANCING EARTH AND SPACE SCIENCES

Geophysical Research Letters

RESEARCH LETTER
10.1029/2025GL117274

Persistent 2024 Warm-Season Marine Heatwave in the Kuroshio Extension Region Under Global Warming

Lifei Qiao[1,2], **Haosu Tang**[3], **and Gang Huang**[1,2]

[1]State Key Laboratory of Earth System Numerical Modeling and Application, Institute of Atmospheric Physics, Chinese Academy of Sciences, Beijing, China, [2]University of Chinese Academy of Sciences, Beijing, China, [3]School of Geography and Planning, University of Sheffield, Sheffield, UK

Key Points:

- The 2024 Kuroshio Extension marine heatwave was driven by both anticyclonic eddies and increased shortwave radiation
- The Rossby wave train induced by North Atlantic sea surface temperature anomalies reinforced the persistent atmospheric blocking
- The 2024 marine heatwave is unlikely without anthropogenic forcing, with ~35% of its intensity attributed to atmospheric circulation

Supporting Information:

Supporting Information may be found in the online version of this article.

Correspondence to:

H. Tang and G. Huang,
haosu.tang@sheffield.ac.uk;
hg@mail.iap.ac.cn

Citation:

Qiao, L., Tang, H., & Huang, G. (2025). Persistent 2024 warm-season marine heatwave in the Kuroshio extension region under global warming. *Geophysical Research Letters*, *52*, e2025GL117274. https://doi.org/10.1029/2025GL117274

Received 27 MAY 2025
Accepted 6 AUG 2025

Author Contributions:

Conceptualization: Haosu Tang
Data curation: Lifei Qiao
Formal analysis: Lifei Qiao, Haosu Tang
Funding acquisition: Gang Huang
Investigation: Lifei Qiao
Methodology: Lifei Qiao, Haosu Tang
Project administration: Gang Huang
Resources: Lifei Qiao
Software: Lifei Qiao
Supervision: Haosu Tang, Gang Huang
Validation: Lifei Qiao
Visualization: Lifei Qiao
Writing – original draft: Lifei Qiao
Writing – review & editing: Lifei Qiao, Haosu Tang, Gang Huang

Abstract In 2024, the Kuroshio Extension (KE) region experienced a prolonged marine heatwave (MHW), intensifying during the warm season and peaking in mid-August. Mixed-layer heat budget analysis reveals that the onset was primarily driven by anticyclonic eddies associated with a northward-shifted KE axis and enhanced shortwave radiation due to atmospheric blocking. This was further amplified by an eastward-propagating Eurasian teleconnection wave train triggered by North Atlantic sea surface temperature (SST) anomalies. The decay phase was dominated by eddy activity and wind–evaporation–SST feedback. Attribution analysis shows that such an event would have been unlikely without anthropogenic forcing, with approximately 35% of its magnitude attributed to atmospheric circulation, and the remaining 65% to thermodynamic warming and oceanic internal dynamics. These results highlight the increasing likelihood of persistent MHWs in dynamic western boundary current regions under climate change, emphasizing the need for enhanced predictive tools and targeted adaptation efforts.

Plain Language Summary Marine heatwaves (MHWs), defined as prolonged periods of anomalously warm sea surface temperatures (SST), are increasing in frequency and intensity under climate change. This study examines a persistent MHW that occurred in the Kuroshio Extension (KE) region during the 2024 warm season, maintaining strong intensity over an extended duration. During the onset phase, a northward-displaced KE axis generated anticyclonic eddies that transported warm subtropical waters northeastward. Concurrently, reduced cloud cover induced by an atmospheric blocking enhanced shortwave radiation, intensifying surface warming. This was further linked to an eastward-propagating Eurasian Rossby wave train triggered by North Atlantic SST anomalies. In the decay phase, anomalous westerly winds enhanced latent heat loss and suppressed warming through wind–evaporation–SST feedback. Attribution analysis indicates that approximately 35% of the event's intensity can be attributable to atmospheric circulation anomalies, while the remaining 65% is linked to anthropogenic warming and oceanic internal dynamics. These results highlight the combined roles of oceanic and atmospheric processes in driving MHWs in western boundary current regions. Improved understanding of these mechanisms is essential for enhancing prediction capabilities and informing early warning and adaptation strategies under continued climate change.

1. Introduction

Marine heatwaves (MHWs) are extreme oceanic events characterized by prolonged periods of exceptionally warm sea surface temperatures (SSTs), lasting from several days to months or even longer (Hobday et al., 2016). These extreme events have far-reaching ecological and economic consequences, including widespread coral bleaching, reduced seagrass density, and significant declines in kelp biomass (Oliver et al., 2018; Smale et al., 2019). In 2024, global SSTs exceed the 2023 annual mean by 0.05°C–0.07°C, and the upper 2000 m ocean heat content reach record-breaking levels (Cheng et al., 2025). Meanwhile, satellite observations from the National Oceanic and Atmospheric Administration (NOAA) reveal that approximately 77% of the world's coral reefs, spanning the Atlantic, Pacific, and Indian Oceans, have been exposed to bleaching-level heat stress driven by record-breaking ocean temperatures fueled by anthropogenic climate change. These alarming trends underscore the urgency of improving our understanding of MHW dynamics, including their spatiotemporal characteristics and physical drivers, to inform effective climate adaptation and mitigation strategies.

The Kuroshio Extension (KE) region, a prominent western boundary current system in the Northern Hemisphere, is particularly susceptible to prolonged and intense MHWs. Characterized by strong SST variability and a

relatively shallow mixed layer (typically less than 40 m), the KE region responds rapidly to atmospheric forcing, making it a hotspot for extreme ocean warming. Previous studies have shown that KE MHWs arise from a combination of large-scale climate variability and local ocean–atmosphere dynamics. For instance, the summer 2021 event in the Northwest Pacific (NWP) was linked to a northward shift of the KE axis, enhanced anticyclonic eddy activity, and decadal warming trends in the preceding winter that preconditioned both sea surface height (SSH) and temperature anomalies (Du et al., 2022; Kuroda & Setou, 2021). Other studies emphasize the role of basin-scale teleconnections, such as Pacific Decadal Variability and El Niño, and local feedback involving surface heat fluxes, mixed-layer stratification, and eddy-driven advection (Oh et al., 2024; Qiao et al., 2025; Tan et al., 2023). These multifaceted drivers highlight the need for integrated atmospheric–oceanic analysis to disentangle the respective roles of atmospheric and oceanic dynamics in MHW events over the KE region.

The Intergovernmental Panel on Climate Change (IPCC) Sixth Assessment Report (AR6) indicates that anthropogenic climate change has been the primary driver of increasing frequency and intensity of MHWs, with 84%–90% of those recorded between 2006 and 2015 attributable to human-induced warming (IPCC, 2021). Several event attribution studies have been conducted over the KE region. For example, the July 2021 KE MHW is found to be closely associated with mean climate warming, with anthropogenic activities increasing its likelihood by approximately 43-fold (Li et al., 2023). Likewise, the unprecedented compound land–ocean heatwave of summer 2021 across the KE region has become about 30-times more probable due to human-induced warming. Under a moderate emission scenario, its risk in the latter half of the 21st century is projected to be at least six times higher than in the 2020s (Tang et al., 2023). Han et al. (2022) also point out that anthropogenic forcing has significantly contributed to sea level height extremes and compound height–heat extremes along the Indian Ocean coast of Indonesia. During the negative phase of the Indian Ocean Dipole, coinciding with La Niña, weakened southwesterly monsoon winds elevate sea levels and deepen the thermocline, creating favorable conditions for extensive MHWs. This highlights the critical interplay between anthropogenic warming and natural climate variability in shaping regional MHW development.

Throughout 2024, a record-breaking MHW persisted in the KE region, yet the underlying mechanisms driving its formation and longevity remain unclear. Understanding the key processes governing this event is crucial for improving prediction skill, assessing future risks under global warming, and informing strategies to mitigate its ecological and socio-economic impacts. The key research questions this study seeks to address are: (a) What are the spatiotemporal characteristics of this MHW event? (b) What physical mechanisms underpin the evolution of this event? (c) To what extent does anthropogenic forcing contribute to the intensity of this event? The rest of this paper is structured as follows. Section 2 outlines the data and methods. Section 3 presents the characteristics of the event, explores its potential physical mechanisms, and provides attribution and projection results. Section 4 offers conclusion and discussions, including implications for future KE MHWs.

2. Data and Methods

2.1. Reanalysis and Model Data

In this study, we analyze the characteristics of MHWs in the KE region during the warm reason (May–September, MJJAS) of 2024. The observed daily SST data are acquired from the NOAA Optimum Interpolation SST version 2 (OISST v2) High Resolution Data set (Huang et al., 2021), with a spatial resolution of 0.25° × 0.25°. The atmospheric variables, including daily geopotential height (HGT) and horizonal wind fields, are sourced from the National Centers for Environmental Prediction–Department of Energy (NCEP–DOE) Reanalysis II data set. These data have a horizontal resolution of 2.5° × 2.5° and extend from January 1979 to the present (Kanamitsu et al., 2002). The total cloud cover and evaporation data are obtained from the fifth-generation European Center for Medium-Range Weather Forecasts (ECMWF) reanalysis (ERA5) (Hersbach et al., 2023), with the horizontal resolution of 0.25° × 0.25°. To investigate the physical drivers of 2024 MHW event, we analyze concurrent changes in key atmospheric and oceanic variables, including Upward Longwave Radiation Flux , Downward Longwave Radiation Flux, Upward Shortwave Radiation Flux, Downward Shortwave Radiation Flux, Sensible Heat Flux, Latent Heat Flux (LHF), zonal (u) and meridional (v) components of ocean current, and seawater potential temperature. The daily radiation and heat flux data are obtained from the Japanese Reanalysis for Three Quarters of a Century (JRA-3Q) with a spatial resolution of 0.375° × 0.375°, which provides long-term coverage dating back to September 1947 (Naoe et al., 2025). The daily ocean mixed layer thickness, SSH, u and v components of ocean current and seawater potential temperature are retrieved from the Copernicus Marine

Environment Monitoring Service (CMEMS) GLORYS12V1 Reanalysis. This data set provides high-resolution (1/12°) daily subsurface ocean temperature and salinity fields covering the satellite altimetry period from 1993 to the present. The daily sea level anomaly data set estimated by Optimal Interpolation with a spatial resolution of 25 km is provided by the AVISO product from CMEMS.

To investigate the impact of anthropogenic forcing on the intensity of the 2024 MHW event, we employ an attribution framework based on the Canadian Earth System Model version 5 (CanESM5) (Swart et al., 2019), which is a fully coupled earth system model that forms part of the Coupled Model Intercomparison Project Phase 6 (CMIP6). Two sets of large-ensemble simulations are included: (a) the historical ensemble (ALL), comprising 50 members spanning 1965–2014, driven by both natural (solar activity and volcanic aerosols) and anthropogenic forcings; and (b) the hist-nat ensemble (NAT), also consisting of 50 members over the same period but forced solely by natural forcings. To assess the future occurrence of MHWs like that of 2024, we analyze projections under four Tier-1 Shared Socioeconomic Pathways (SSP1-2.6, SSP2-4.5, SSP3-7.0, and SSP5-8.5) across three future periods: near-term (2021–2040), mid-term (2041–2060), and long-term (2081–2100) (IPCC AR6, 2023). In view of the climatological baseline for 1994–2023, the ALL simulation is extended to 2023 under the framework of the SSP2-4.5 scenario. Considering potential model biases, we apply a delta bias correction to the CanESM5 simulations to align the model's climatology more closely with observations, thereby improving the reliability of the attribution results. All data sets have been interpolated onto a uniform $1° \times 1°$ horizontal grid to ensure consistency before formal analysis.

2.2. MHW Definition

MHWs in this study are identified based on SST exceeding the 90th percentile threshold of a 30-year historical reference period (1994–2023). The selection of 1994 as the starting year is primarily due to the availability of high-resolution subsurface ocean temperature observations. To reduce short-term variability, we smooth SST using a 5-day running mean, and an event is classified as an MHW if it persists for at least five consecutive days (Hobday et al., 2016). MHWs are further categorized based on multiples of the local difference between the climatology and the 90th percentile threshold: moderate (1–2×, Category I), strong (2–3×, Category II), severe (3–4×, Category III), and extreme (>4×, Category IV) (Hobday et al., 2018). The onset phase of an MHW is defined as the period between the initiation and the peak of the event, whereas the decay phase refers to the period from the peak until the event's termination.

To comprehensively assess MHW characteristics, we employ the cumulative magnitude index (CMI), which integrates the intensity, duration, and frequency of MHWs, facilitating comparative analysis across different spatial and temporal scales (Qiao et al., 2025). The CMI is defined as follows:

$$\mathrm{CMI} = \sum_{i=1}^{n} \sum_{d=1}^{d_i} T_{(i,d)} \tag{1}$$

where n denotes the total number of MHW events within the warm season of each year, and d_i represents the duration of the ith MHW event. $T_{(i,d)}$ corresponds to the difference between SST and the threshold on day d of the ith event, with the value set to zero when no MHWs occur. By calculating intensity relative to this threshold, the CMI captures only temperature anomalies exceeding the event-defining baseline, providing a consistent and meaningful measure of MHW intensity.

2.3. Other Statistical Methods

To elucidate the co-variability between the KE and North Atlantic (NA) regions, we employ the singular value decomposition (SVD) to the cross-covariance matrix of detrended SST anomalies (SSTA) (Bretherton et al., 1992). The two-tailed Student's t-test is applied to evaluate the statistical significance of the derived spatial patterns. Moreover, the kernel density estimation (KDE) is employed to estimate the probability density function (PDF) of SST. Additionally, we apply the two-sample Kolmogorov–Smirnov (K–S) test to assess whether the SST distributions of two independent samples differ significantly. To examine the impact of specific SST patterns, we categorize 2500 ensemble members from the historical experiment (1965–2014) of CanESM5 based on their correlation with the target SST index. Members exhibiting a statistically significant correlation coefficient

above 0.5 ($p < 0.01$) are classified as strong positive cases, whereas those with a coefficient below −0.5 are identified as strong negative cases.

In this study, the KE axis is identified following the method of Nakano et al. (2018). Specifically, for each day, we compute surface velocity values along every SSH contour using data from the CMEMS GLORYS12V1 ocean reanalysis. The location of maximum velocity is then determined, and the SSH contour corresponding to this location is designated as the KE axis for that day. The daily KE latitude is subsequently defined as the mean latitudinal position of this axis within the longitudinal band from 140°E to 160°E.

To quantify the relative contributions of atmospheric circulation to the 2024 KE MHW, we further apply the flow analog method. This method isolates the dynamical influence of atmospheric circulation by identifying historical periods with similar large-scale circulation patterns and comparing their associated SSTA to those observed during the event of interest. In this study, the 200 hPa HGT, with the zonal mean removed, is used as the circulation indicator. We then identify the ten most analogous historical circulation patterns to those observed over the KE region during MJJAS 2024, based on Euclidean distance, within the period from 1994 to 2023. Sensitivity tests are conducted by varying the number of analogs (5 and 15) and exploring alternative similarity metrics, including Pearson's correlation, Spearman's rank correlation, and cosine similarity.

3. Results

3.1. An Unusually Long-Lasting MHW During MJJAS 2024

The year 2024 experiences a persistent MHW over the NWP across the entire year, with its intensity becoming particularly pronounced during the warm season. Throughout this period, significant positive SSTA are observed across a vast region of the NWP, with anomalies reaching up to 2°C in the KE region (Figure 1a). Compared to the climatology period, nearly the entire study domain exhibits significantly elevated SSTs, culminating in record-breaking MHW conditions (Figure S1 in Supporting Information S1). The 2024 KE MHW persists continuously from May to September, with peak intensity concentrated along the western and northern flanks of the KE region (Figures S2a and S2b in Supporting Information S1). The duration of the event exceeds 60 days in most affected regions (Figure S2c in Supporting Information S1).

Although 2024 is characterized as an El Niño decay year, SSTA in the KE region exhibits only a weak correlation with the preceding winter Niño3.4 index (Figure S3a in Supporting Information S1). In contrast, a strong association with local 850-hPa HGT anomalies indicates that atmospheric forcing may exert an important control over sea surface conditions during this period (Figures S3b–S3d in Supporting Information S1). During the warm season of 2024, an anomalous high-pressure system is centered over subtropical NWP (Figure 1b). The western flank of this high-pressure system exerts a strong influence over the KE region, where westerly wind anomalies dominate the northern sector and easterly anomalies prevail in the south. From a long-term perspective, the raw SSTA over the KE region in 2024 reaches 1.797°C, the highest value recorded since 1982 (Figure 1c). After removing the linear warming trend, the SSTA remains at 0.957°C, ranking as the third highest on record.

In addition to ocean surface warming, record-breaking warmth is also observed in both the atmosphere and subsurface ocean layers. The atmospheric temperature profile over the KE region in 2024 is characterized by an initial temperature increase with altitude up to approximately 920 hPa, followed by a decrease toward 850 hPa, and then a secondary warming layer aloft (Figure S4a in Supporting Information S1). Notably, the lower-tropospheric warming in 2024 exceeds that of previous years throughout the entire lower atmospheric column, reflecting enhanced heat accumulation near the surface. Meanwhile, the mixed layer depth across the KE region remains relatively shallow, generally less than 40 m (Figure S5a in Supporting Information S1). This allows the upper ocean to warm more rapidly. Consequently, anomalously high ocean temperatures penetrate down to approximately 200 m, with the strongest anomalies confined to the surface and gradually decreasing with depth (Figure S4b in Supporting Information S1). Given this vertical structure, SST is selected as the primary variable for MHW analysis in this study.

The 2024 KE MHW peaks on mid-August and persists at Category I (moderate) intensity throughout most of its lifespan (Figure 1d). Based on the evolution of both SST and CMI, 15 August is identified as the point of maximum development. The period from the initial development to the peak intensity of the MHW is defined as the onset phase, while the interval from the peak to the event's termination is referred to as the decay phase.

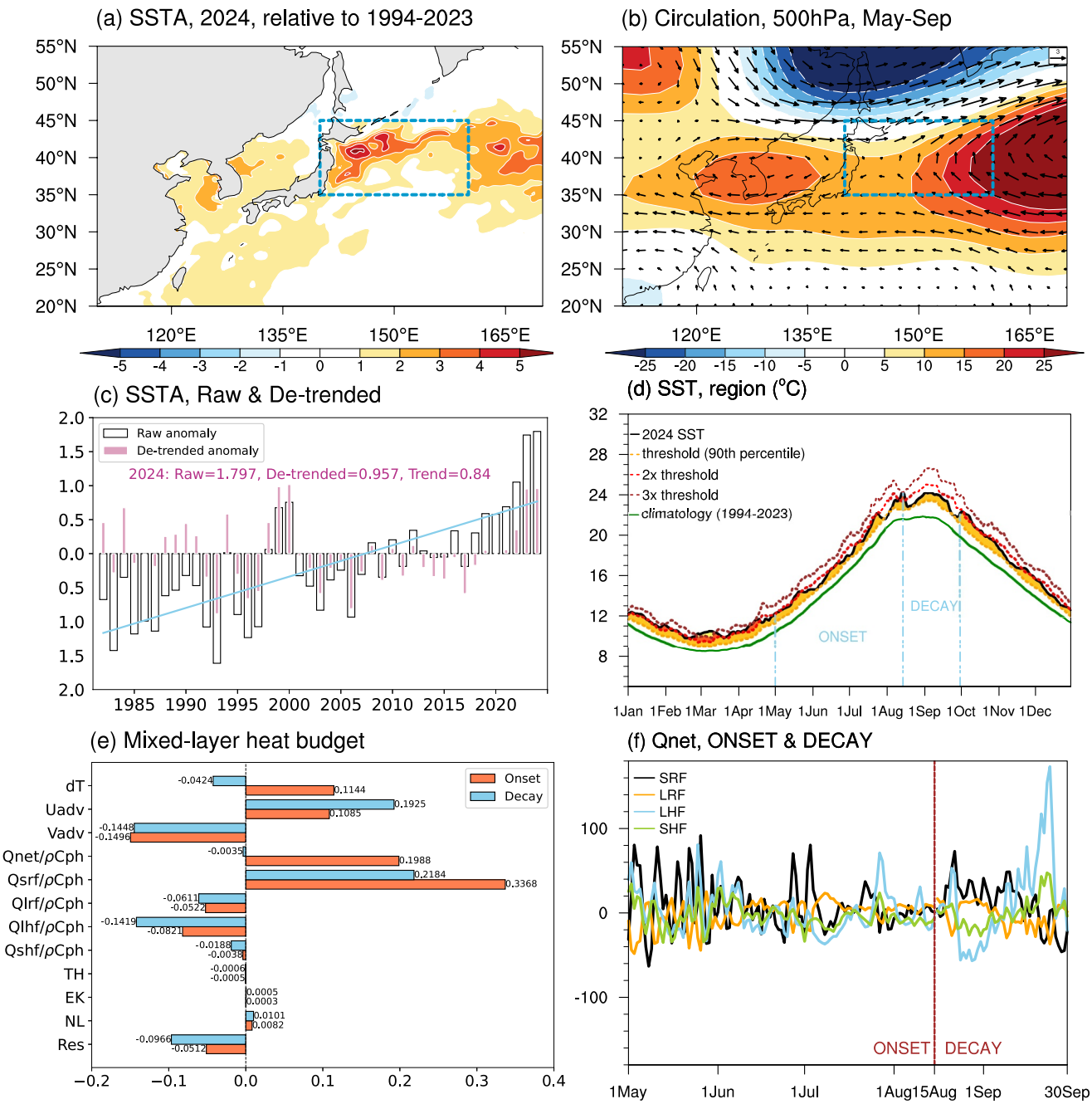

Figure 1. (a) Spatial distribution of SSTA (°C, shading) during MJJAS 2024. The blue box (35°–45°N, 140°–160°E) delineates the KE region analyzed in this study. (b) Anomalies of 500-hPa eddy geopotential height (gpm, shading) and winds (m/s, vectors) during MJJAS 2024. (c) Time series of KE-averaged SSTA (black bars), linear trend (blue line), and detrended anomalies (pink bars) during MJJAS from 1982 to 2024. (d) Daily sea surface temperature (SST) evolution in 2024 (°C, black), along with the climatological mean SST (°C, green), and the 90th percentile threshold of the 5-day running mean SST (°C, orange dashed line) used to define Category I (moderate) MHWs. Red and brown dashed lines indicate thresholds for Category II (strong) and Category III (severe) MHWs, respectively. The color shading beneath the SST curve denotes the MHW category for each day. The onset and decay phases of the 2024 MHW event are labeled in blue. (e) Bar chart of mixed-layer heat budget terms (°C/day) during the onset (orange) and decay (blue) phases of the 2024 KE MHW, including the temperature tendency (dT), zonal and meridional advection (Uadv, Vadv), Q_{net}, Q_{SRF}, Q_{LRF}, Q_{LHF}, Q_{SHF}, thermocline feedback (TH), upwelling feedback (EK), nonlinear (NL), and the residual term (Res). (f) Daily evolution of surface heat flux component anomalies (W/m^2): Q_{SRF} (black), Q_{LRF} (orange), Q_{LHF} (blue), and Q_{SHF} (green) during MJJAS 2024.

During the onset phase, the MHW intensifies rapidly, with brief but extreme phase of Category II (strong) level occurring in late May and mid-August. However, this extreme phase is short-lived and quickly subsides (Figure 1d).

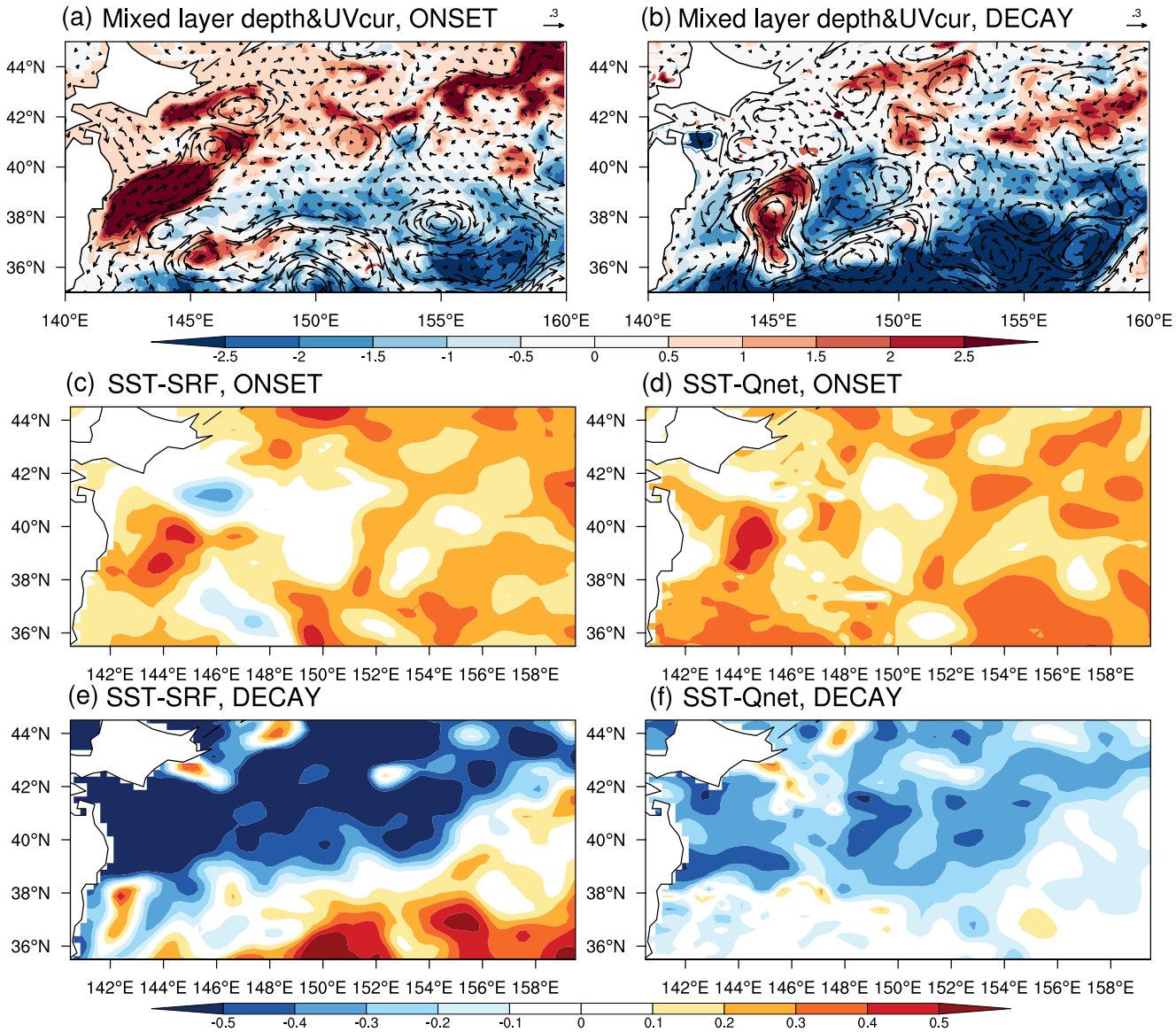

Figure 2. Anomalies of the upper-ocean current (vectors) and mixed layer depth (shading) in the (a) onset and (b) decay phase relative to the 1994–2023 climatology during MJJAS 2024. Simultaneous correlation of SST–SRF and SST–Qnet during (c, d) the onset phase and (e, f) the decay phase in MJJAS 2024. Positive values indicate that higher sea surface temperatures are associated with enhanced downward fluxes.

3.2. Mixed Layer Heat Budget Analysis

To understand the evolution of the 2024 KE MHW, we first examine its potential drivers by analyzing the time-dependent evolution of each term in the mixed-layer heat budget (Text S1 in Supporting Information S1). The physical mechanisms governing the event exhibit distinct characteristics between the onset and decay phases. During the onset phase, the primary contributors are Uadv and Qnet, while the decay phase is predominantly influenced by LHF, Vadv, and horizontal eddy heat fluxes (Res) (Figure 1e). During the onset phase, pronounced positive values of Uadv indicate an influx of warm seawater from the zonal direction. The extreme northward displacement of the KE axis (Figure S5b in Supporting Information S1) results in the generation of anticyclonic eddies that deepen the mixed layer while simultaneously advecting warm subtropical waters northeastward along the western boundary (Figure 2a). This substantial heat transport, together with the intensified western boundary current, facilitates the maintenance and development of positive SSTA. These processes become increasingly significant as the mixed layer deepens, particularly in late summer (Oh et al., 2024). Additionally, the SRF exhibits significant temporal variability, exerting a pronounced warming effect (Figure 1f). Enhanced shortwave

radiation, driven by diminished low-level cloud cover (Figure S7a in Supporting Information S1), outweighs the cooling effects of other heat flux anomalies across most of the study domain (Figure S6a in Supporting Information S1). Meanwhile, the KE region lies west of the anomalous atmospheric high-pressure system, where southerly wind anomalies transport warm and moist air from the subtropics. This sustained advection of heat and moisture also helps maintain persistently warm and humid conditions in the lower troposphere.

During the decay phase, the LHF exhibits a pronounced negative anomaly, with a sharp increase since September, while the SRF remains consistently positive (Figure 1f). In the northwest KE region, the anomalous westerlies strengthen the background wind field (Figure 1b), thereby enhancing surface evaporation (Figure S8b in Supporting Information S1). This increased latent heat release promotes sea surface cooling via wind–evaporation–SST (WES) feedback (Figure S6g in Supporting Information S1). Additionally, the southward shift of the KE axis (Figure S5b in Supporting Information S1) is accompanied by a weakening of anticyclonic eddies to the north and a progressive intensification of cyclonic eddies to the south (Figure S9 in Supporting Information S1), resulting in widespread shoaling of the mixed layer in the southern sector. Concurrently, meridional heat transport along the western boundary is markedly diminished, ultimately leading to the attenuation of MHWs (Figure 2b).

From another perspective on the observed SST anomalies, the spatial patterns of SST–SRF and SST–Qnet correlations closely match each other in both phases, underscoring the key role of shortwave radiation in modulating SSTA (Figures 2c–2f). During the onset period, strong positive correlation between SST and SRF pervades nearly the entire study area, likely attributable to cloud–radiation feedback. Specifically, reduced cloud cover amplifies shortwave radiation, thereby facilitating SST augmentation (Figure 2c). Conversely, in the decay phase, SST–SRF correlations become strongly negative, particularly along the western and northern margins where anomalous high-pressure systems exert a more pronounced influence (Figure 2e). Here, elevated SSTs induce an increase in cloud cover, consequently diminishing SRF, while oceanic advection dominates the subsequent SST decline.

3.3. Atlantic Origin of the KE Blocking High

Although the atmospheric blocking high has been identified as the key driver of the 2024 KE MHW, a critical question arises: what physical mechanisms are responsible for driving this localized circulation anomaly? To address this, we first regress SSTA in the Northern hemisphere onto an index of KE-region SSTA, which reveals a significant warming center over the NA (40°N–60°N, 70°W–40°W) (Figure 3a). To validate this relationship, we apply SVD to SSTA fields over the KE and NA regions. The leading SVD mode explains 66.73% of the total variance, with coherent positive signals across both regions. The principal components correlate at $r = 0.68$, and both reach high values during 2024, indicating a strong statistical link (Figures 3c–3f).

To further establish the dynamical pathway, we compute the Rossby wave source (RWS) at 200 hPa. The pronounced positive NA SSTA intensify upper-level outflow, thereby facilitating the development of negative RWS, indicative of anomalous upper-tropospheric divergence capable of triggering a Rossby wave train (Figure S10 in Supporting Information S1). We then examine the 200-hPa eddy geopotential height anomalies (HGT anomalies with the zonal mean removed) and corresponding horizontal wave-activity fluxes. The results indicate a Rossby wave train emanating from the NA region, propagating across the Eurasian continent, and culminating in an anticyclonic anomaly over the KE region (Figure 3b). Along its trajectory, alternating high- and low-pressure anomalies appear in succession, forming a coherent wave pattern. The anticyclonic anomaly over Northeast Asia propagates northward toward the Bering Strait, where it evolves into a cyclonic anomaly. This anomaly subsequently extends southward, establishing a robust anticyclonic system over the KE region. This influence of NA SSTA on Eurasian atmospheric circulation and regional climate anomalies is also documented in previous observational studies and numerical simulations (Chen et al., 2021; Meng & Gong, 2022).

Beyond observational analyses, we further employ the CanESM5 model to substantiate the linkage between NA and KE SSTA. Composite maps for strong positive and negative NA SSTA, constructed from a 2500-member ensemble (1965–2014) sorted by the NA SSTA index, reveal contrasting KE responses (Figures 4a and 4b). Under positive NA SSTA, KE SSTs warm substantially, especially in the northern sector. Likewise, negative NA SSTA are associated with substantial SST cooling over the KE region, again most markedly in the north. These patterns further validate the mechanism whereby NA warming triggers Rossby wave trains that establish local blocking highs favoring KE warming.

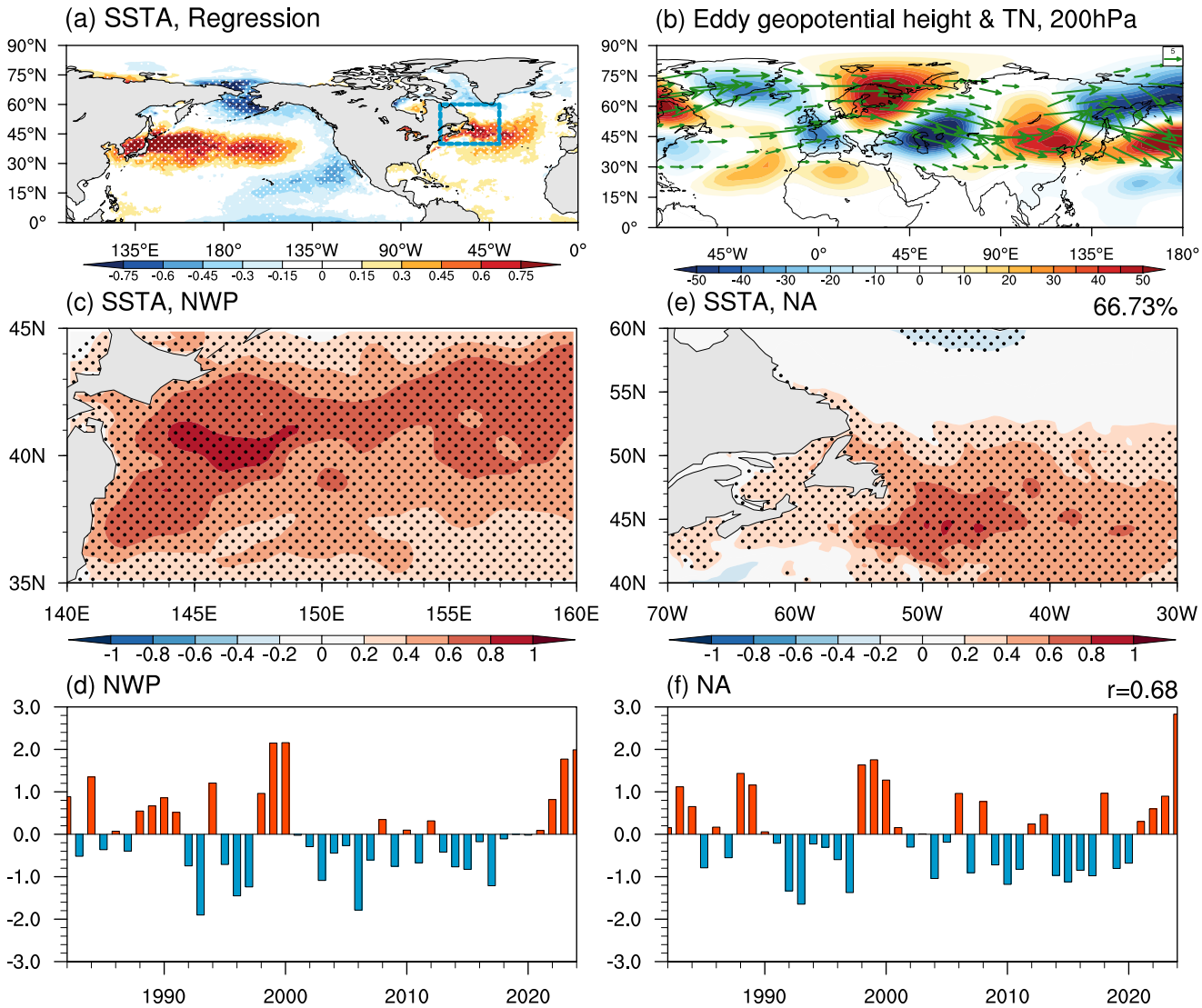

Figure 3. (a) Regression of SSTA (°C, shading) in the Northern Hemisphere onto the area-averaged SSTA in the KE region during MJJAS for the period 1982–2024. The blue box outlines the NA region analyzed in this study. (b) 200-hPa eddy geopotential height anomalies (gpm, shading) and the corresponding wave activity flux (m^2/s, vectors) during MJJAS 2024. (c, e) Spatial patterns of the first leading SVD coupled modes of detrended SSTA over NWP and NA, respectively. Dotted areas indicate regions where the anomalies are statistically significant at the 95% confidence level. (d, f) Corresponding standardized time series of the SVD mode pairs shown in (c) and (e), respectively.

3.4. Anthropogenic Influence on the 2024 Event

Beyond local and remote drivers, we further investigate the role of anthropogenic forcing in the 2024 KE MHW. In the early 20th century, both ALL and NAT-only simulations yield similar SSTs stabilizing around 16°C. After the 1980s, however, ALL simulations diverge sharply from NAT, reproducing the observed warming trend while NAT-only simulations remain nearly flat (Figure 4c). This contrast implicates anthropogenic climate change as the primary driver of KE background SST warming. Since the regional-mean SSTA of the 2024 KE MHW far exceed the range of variability in NAT-only simulations, it indicates that such an event would have been virtually impossible without human-induced climate change (Figure 4d).

To quantify the dynamical role of atmospheric circulation, we apply the flow analog method. Figure 4e compares the distribution of KE-averaged SSTA for randomly selected years versus those with analogous 200-hPa circulation patterns (1994–2023). The analog years exhibit markedly higher SSTA (median = 0.63°C), indicating that the anomalous anticyclonic circulation plays a contributory role in the 2024 KE MHW. Accordingly, it is

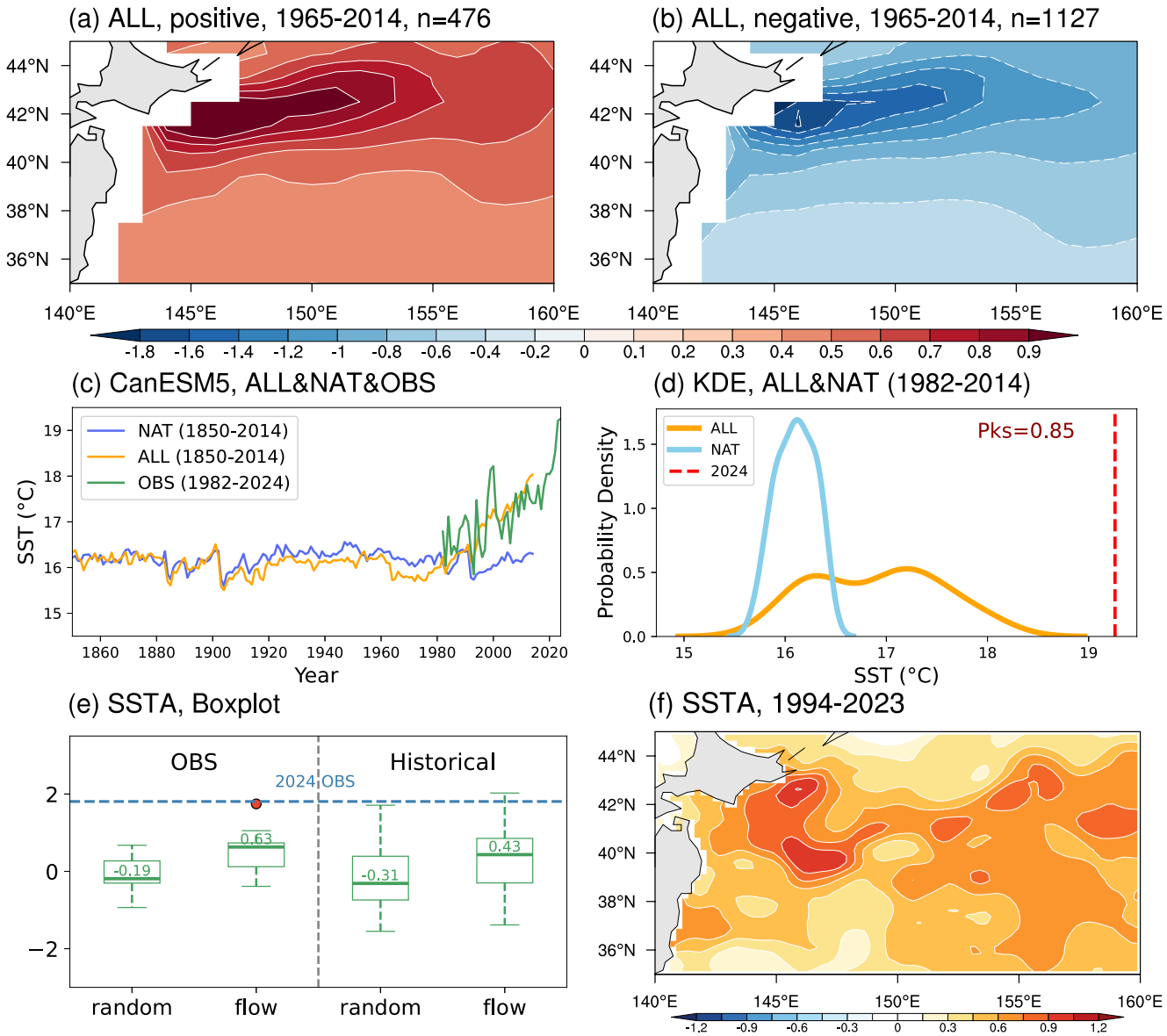

Figure 4. (a, b) Composite spatial patterns of KE SSTA associated with pronounced positive (a) and negative (b) SSTA in the NA. (c) Time series of the observed and simulated MJJAS sea surface temperature (SST) averaged over the KE region (°C). Orange and blue lines represent the ensemble means from CanESM5 historical simulations with all forcings (ALL) and natural forcings only (NAT) during 1850–2014, respectively. (d) Probability density functions (PDFs) of SST averaged over the KE region from CanESM5 simulations under ALL (orange) and NAT (blue) forcings. The vertical red dashed line indicates the observed SST in 2024. (e) Distributions of KE regional averaged SSTA (°C) for randomly selected years (first and third boxplots) and for years identified via the flow analog method (second and fourth boxplots), based on observations and CanESM5 historical simulations during 1994–2023. The boxplot shows the 25th percentile, median, and 75th percentile (bottom to top), while the horizontal blue dashed line marks the 2024 event threshold. (f) Composite spatial distribution of SSTA (°C) during the flow analog years in the observations, indicating typical patterns associated with similar atmospheric circulation to that in 2024.

estimated that dynamical atmospheric circulation anomalies account for ~35% of the event's intensity, while the remaining 65% arises from the thermodynamic response directly induced by anthropogenic warming and oceanic internal dynamics (Figure 4e). The ten most analogous circulation composites accurately reproduce positive KE SSTA patterns, especially significant warming along the western and northern flanks, which closely mirror 2024 observations (Figure 4f). To further validate these findings, we conduct a sensitivity analysis using cosine similarity as the metric for circulation pattern matching, yielding a median SSTA of 0.46°C. This approach reinforces the conclusion that the contribution of dynamical forcing to the event is comparatively small, while thermodynamic forcing and oceanic internal dynamics predominates (Figure S11a in Supporting Information S1). Additionally, the composite based on the ten most analogous circulation patterns also displays a strong spatial

agreement with the observed 2024 SSTA distribution (Figure S11b in Supporting Information S1), further confirming the robustness of attribution results.

To further evaluate the robustness of conclusions derived from the observations, we apply the same flow analog method to 1,500 ensemble members from the CanESM5 model over the period 1994–2023. The identified analog years consistently show elevated SSTA patterns, with a median anomaly of 0.43°C, indicating that the atmospheric dynamical contribution accounts for less than 50% (Figure 4e). Additional support for the dominant role of thermodynamic forcing and oceanic internal dynamics comes from the 20 most analogous circulation composites, which reveal a predominantly positive SSTA field. The anomalies are strongest in the northern KE and broadly consistent with the observed distribution in 2024 (Figure S11c in Supporting Information S1).

Finally, we examine future SST projections across different scenarios and time periods to assess the evolving risk of 2024-like MHWs (Figure S12 in Supporting Information S1). In the short-term future, SST distributions are similar across various SSP scenarios. By the mid and late century, however, SSP5-8.5 scenario yields significant mean warming and a pronounced right skew, indicating both higher SSTs and greater variability. While 2024-like events may still occur under low-emission futures in the near term, their intensity is projected to far exceed the 2024 benchmark by mid-to late century, highlighting an accelerating trend toward more frequent and severe MHWs in the future.

4. Conclusion and Discussions

The 2024 warm-season MHW in the KE region persists for over 153 days with SSTA exceeding 2°C, making it one of the longest and most intense events on record in the region. This study investigates its physical drivers and the role of anthropogenic forcing in this event. The results indicate that the onset of the event is primarily driven by anticyclonic eddies and enhanced northeastward heat transport linked to the northward shift of the KE axis, as well as reduced cloud cover that increases downward shortwave radiation due to anomalous atmospheric blocking. Together, these processes trigger rapid surface warming. In contrast, the decay phase is governed by vertical enhanced latent heat loss via the WES feedback, and eddy activity, as reflected in the shift from positive to negative SST–SRF correlations. Remote forcing emerges as a potential precursor to the KE blocking high that sustains the MHW. Specifically, positive NA SSTA generate negative RWS at 200 hPa and launch an eastward-propagating Rossby wave train. This wave train traverses Eurasia and reinforces the KE blocking high, prolonging the local MHW. CanESM5 large ensemble confirms that natural variability alone cannot reproduce the post-1980s warming trend or the 2024 anomaly. Flow analog analysis attributes approximately 35% of the 2024 KE MHW's intensity to anomalous atmospheric circulation, and the remaining 65% to thermodynamic warming and oceanic internal dynamics.

Western boundary current systems like the KE are among the most energetic and variable regions in the global ocean. Their intense temperature gradients, strong eddy fields, and sensitivity to both natural variability and anthropogenic forcing make them hotspots for ocean–atmosphere interactions, with implications that extend far beyond the local scale. Sustained MHW events in the KE region can disrupt biological productivity, alter large-scale ocean circulation, and even influence North Pacific storm tracks and tropical cyclone formation. This study underscores the joint roles of oceanic and atmospheric processes in triggering and modulating local MHWs, highlighting the need for integrated analysis of coupled dynamics. Future efforts should prioritize high-resolution coupled models and sustained observational programs in the KE region to better resolve the fine-scale dynamics that govern local MHWs, and to enhance the effectiveness of early warning systems, fisheries management, and climate adaptation strategies.

Conflict of Interest

The authors declare no conflicts of interest relevant to this study.

Data Availability Statement

All data used in this study are publicly accessible. The NOAA OISST v2 High Resolution Data set is available at Huang et al. (2021). The NCEP–DOE Reanalysis II data set can be found in Kanamitsu et al. (2002). The daily radiation and heat flux data are based on the JRA-3Q data set (Naoe et al., 2025). The daily total cloud cover and

evaporation data are obtained from ERA5 (Hersbach et al., 2023). The daily sea level anomaly data is accessed from CMEMS AVISO product, available at https://doi.org/10.48670/moi-00148. The daily ocean mixed layer thickness, ocean currents and seawater potential temperature are downloaded from the CMEMS GLORYS12V1 Reanalysis, available at https://doi.org/10.48670/moi-00021. The NCEP GODAS data set is available at Behringer et al. (1998). The CanESM5 model outputs archived in CMIP6 analyzed in this study can be found in Swart et al. (2019).

Acknowledgments
We sincerely appreciate the valuable feedback from the anonymous reviewers, which has significantly enhanced the quality of this manuscript. The authors appreciate the fundings from the National Natural Science Foundation of China (42141019 and 42261144687).

References

Behringer, D. W., Ji, M., & Leetmaa, A. (1998). An improved coupled model for ENSO prediction and implications for ocean initialization. Part I: The ocean data assimilation system [Dataset]. *Monthly Weather Review*, *126*(4), 1013–1021. https://doi.org/10.1175/1520-0493(1998)126<1013:AICMFE>2.0.CO;2

Bretherton, C. S., Smith, C., & Wallace, J. M. (1992). An intercomparison of methods for finding coupled patterns in climate data. *Journal of Climate*, *5*(6), 541–560. https://doi.org/10.1175/1520-0442(1992)005<0541:AIOMFF>2.0.CO;2

Chen, S. F., Wu, R. G., & Chen, W. (2021). Influence of North Atlantic sea surface temperature anomalies on springtime surface air temperature variation over Eurasia in CMIP5 models. *Climate Dynamics*, *57*(9–10), 2669–2686. https://doi.org/10.1007/s00382-021-05826-5

Cheng, L., Abraham, J., Trenberth, K. E., Reagan, J., Zhang, H. M., Storto, A., et al. (2025). Record high temperatures in the ocean in 2024. *Advances in Atmospheric Sciences*, *42*(6), 1092–1109. https://doi.org/10.1007/s00376-025-4541-3

Du, Y., Feng, M., Xu, Z., Yin, B., & Hobday, A. J. (2022). Summer marine heatwaves in the Kuroshio-Oyashio extension region. *Remote Sensing*, *14*(13), 2980. https://doi.org/10.3390/rs14132980

Han, W., Zhang, L., Meehl, G. A., Kido, S., Tozuka, T., Li, Y., et al. (2022). Sea level extremes and compounding marine heatwaves in coastal Indonesia. *Nature Communications*, *13*(1), 6410. https://doi.org/10.1038/s41467-022-34003-3

Hersbach, H., Comyn-Platt, E., Bell, B., Berrisford, P., Biavati, G., Horányi, A., et al. (2023). ERA5 post-processed daily-statistics on pressure levels from 1940 to present [Dataset]. *Copernicus Climate Change Service (C3S) Climate Data Store (CDS)*. https://doi.org/10.24381/cds.4991cf48

Hobday, A. J., Alexander, L. V., coaed, Smale, D. A., Straub, S. C., Oliver, E. C., et al. (2016). A hierarchical approach to defining marine heatwaves. *Progress in Oceanography*, *141*, 227–238. https://doi.org/10.1016/j.pocean.2015.12.014

Hobday, A. J., Oliver, E. C. J., Sen Gupta, A., Benthuysen, J. A., Burrows, M. T., Donat, M. G., et al. (2018). Categorizing and naming marine heatwaves. *Oceanography*, *31*(2), 162–173. https://doi.org/10.5670/oceanog.2018.205

Huang, B., Liu, C., Banzon, V., Freeman, E., Graham, G., Hankins, B., et al. (2021). Improvements of the daily optimum interpolation sea surface temperature (DOISST) version 2.1 [Dataset]. *Journal of Climate*, *34*(8), 2923–2939. https://doi.org/10.1175/JCLI-D-20-0166.1

Intergovernmental Panel on Climate Change (IPCC). (2021). *Climate change 2021: The physical science basis. Contribution of working group I to the sixth assessment report of the intergovernmental panel on climate change*. Cambridge University Press. Retrieved from https://www.ipcc.ch/report/ar6/wg1/

Kanamitsu, M., Ebisuzaki, W., Woollen, J., Yang, S.-K., Hnilo, J. J., Fiorino, M., & Potter, G. L. (2002). NCEP-DOE AMIP-II reanalysis (R-2) [Dataset]. *Bulletin America Meteorology Social*, *83*(11), 1631–1643. https://doi.org/10.1175/BAMS-83-11-1631

Kuroda, H., & Setou, T. (2021). Extensive marine heatwaves at the sea surface in the Northwestern Pacific Ocean in summer 2021. *Remote Sensing*, *13*(19), 3989. https://doi.org/10.3390/rs13193989

Li, D., Chen, Y., Qi, J., Zhu, Y., Lu, C., & Yin, B. (2023). Attribution of the July 2021 record-breaking Northwest Pacific marine heatwave to global warming, atmospheric circulation, and ENSO. *Bulletin of the American Meteorological Society*, *104*(1), E291–E297. https://doi.org/10.1175/BAMS-D-22-0142.1

Meng, M., & Gong, D. (2022). Winter North Atlantic SST as a precursor of spring Eurasian wildfire. *Geophysical Research Letters*, *49*(18), e2022GL099920. https://doi.org/10.1029/2022GL099920

Nakano, H., Tsujino, H., Sakamoto, K., Urakawa, S., Toyoda, T., & Yamanaka, G. (2018). Identification of the fronts from the Kuroshio Extension to the subarctic current using absolute dynamic topographies in satellite altimetry products [Dataset]. *Journal of Oceanography*, *74*(4), 393–420. https://doi.org/10.1007/s10872-018-0470-4

Naoe, H., Kobayashi, C., Kobayashi, S., Kosaka, Y., & Shibata, K. (2025). Representation of quasi-biennial oscillation in JRA-3Q [Dataset]. *J. Meteor. Soc. Japan*, *103*(2), 233–255. https://doi.org/10.2151/jmsj.2025-012

Oh, H., Chu, J. E., Min, Y., Kim, G. U., Jeong, J., Lee, S., et al. (2024). Late-arriving 2023 summer marine heatwave in the East China Sea and implications for global warming. *npj Clim Atmos Sci*, *7*(1), 294. https://doi.org/10.1038/s41612-024-00846-4

Oliver, E. C. J., Donat, M. G., Burrows, M. T., Moore, P. J., Smale, D. A., Alexander, L. V., et al. (2018). Longer and more frequent marine heatwaves over the past century. *Nature Communications*, *9*(1), 1324. https://doi.org/10.1038/s41467-018-03732-9

Qiao, L., Tang, H., & Huang, G. (2025). Drivers and predictability of summer marine heatwaves in the Northwest Pacific. *Journal of Geophysical Research: Atmospheres*, *130*(6), e2024JD042994. https://doi.org/10.1029/2024jd042994

Smale, D. A., Wernberg, T., Oliver, E. C. J., Thomsen, M., Harvey, B. P., Straub, S. C., et al. (2019). Marine heatwaves threaten global biodiversity and the provision of ecosystem services. *Nature Climate Change*, *9*(4), 306–312. https://doi.org/10.1038/s41558-019-0412-1

Swart, N. C., Cole, J. N. S., Kharin, V. V., Lazare, M., Scinocca, J. F., Gillett, N. P., et al. (2019). The Canadian Earth system model version 5 (CanESM5.0.3) [Dataset]. *Geoscientific Model Development*, *12*(11), 4823–4873. https://doi.org/10.5194/gmd-12-4823-2019

Tan, H.-J., Cai, R.-S., Bai, D.-P., Karim, H., & Kareem, T. (2023). Causes of 2022 summer marine heatwave in the East China Seas. *Advances in Climate Change Research*, *14*(5), 633–641. https://doi.org/10.1016/j.accre.2023.08.010

Tang, H., Wang, J., Chen, Y., Tett, S. F., Sun, Y., Cheng, L., et al. (2023). Human contribution to the risk of 2021 northwestern Pacific concurrent marine and terrestrial summer heat. *Bulletin America Meteorology Social*, *104*(3), E673–E679. https://doi.org/10.1175/bams-d-22-0238.1

References From the Supporting Information

Oliver, E. C. J., Benthuysen, J. A., Darmaraki, S., Donat, M. G., Hobday, A. J., Holbrook, N. J., et al. (2021). Marine heatwaves. *Annual Review of Marine Science*, *13*(1), 313–342. https://doi.org/10.1146/annurev-marine-032720-095144

Takaya, K., & Nakamura, H. (2001). A formulation of a phase-independent wave-activity flux for stationary and migratory quasigeostrophic eddies on a zonally varying basic flow. *Journal of the Atmospheric Sciences*, *58*(6), 608–627. https://doi.org/10.1175/1520-0469(2001)058<0608:afoapi>2.0.co;2